

# Error-correcting one-way quantum computation with global entangling gates

Jaewoo Joo and David L. Feder<sup>1</sup>

<sup>1</sup>*Institute for Quantum Information Science, University of Calgary, Alberta T2N 1N4, Canada*  
(Dated: November 13, 2021)

We present an approach to one-way quantum computation (1WQC) that can compensate for single-qubit errors, by encoding the logical information residing on physical qubits into five-qubit error-correcting code states. A logical two-qubit cluster state that is the fundamental resource for encoded quantum teleportation is then described by a graph state containing ten vertices with constant degree seven. Universal 1WQC that incorporates error correction requires only multiple copies of this logical two-qubit state and a logical four-qubit linear cluster state, which are prepared only just in advance of their use in order to minimize the accumulation of errors. We suggest how to implement this approach in systems characterized by qubits in regular two-dimensional lattices for which entangling gates are generically global operations, such as atoms in optical lattices, quantum dots, or superconducting qubits.

PACS numbers: 03.67.Lx, 03.67.-a, 03.67.Pp

## I. INTRODUCTION

A fundamental requirement for the implementation of reliable quantum information processing is the ability to diagnose the presence of errors that might have occurred on quantum bits (qubits) and to make the appropriate corrections, without obtaining any knowledge of the quantum information itself. Quantum error-correcting codes (QECCs) were developed over a decade ago that can accomplish this [1, 2, 3, 4, 5, 6], with a five-qubit QECC being the smallest that can perfectly protect against an arbitrary error on a single qubit [7, 8, 9]. QECCs serve as a crucial ingredient for fault tolerance [10, 11], which is the full protection of quantum information during the implementation of all quantum gates and measurements, as long as the frequency of errors is below a certain threshold [12, 13]. The usual approach to fault tolerance is through concatenation of QECCs [14], though these generally give very low thresholds [15]; topological approaches to quantum computation can cope in principle with much higher error rates [16, 17]. Many QECC schemes have been successfully demonstrated theoretically and experimentally over the years [18].

It remains unclear how best to extend the ‘one-way’ quantum computation (1WQC) model [19, 20], where processing occurs solely by performing measurements on a highly entangled ‘graph’ state, to include fault tolerance. The most intuitive method, which is to implement an encoded quantum circuit in 1WQC [21, 22, 23], does not directly correct for errors in the preparation of the relevant graph state nor errors that accumulate on physical qubits as a function of time. One approach would be to embed the cluster state in a decoherence-free subspace [24, 25, 26]. Topological techniques [27, 28, 29, 30, 31] solve this problem and yield high error thresholds. A complementary method for fault-tolerant 1WQC that has been recently proposed is based on embedding QECC graphs into the computational graph state [32, 33, 34], and our proposal has some

features in common with these. If the encoded graph state is prepared in advance, however, this approach cannot adequately compensate for the large number of errors that are likely to have occurred on distant physical qubits by the time they are measured.

We propose a simple and practical method for 1WQC that incorporates the five-qubit QECC, which is the minimum size for quantum codes that can correct single-qubit errors, and which has a simple and intuitive construction in terms of graph states. The main approach is two-fold. First, rather than building the full (computational) cluster state in advance, one instead forms a collection of linear two-qubit and four-qubit (sideways ‘horseshoe’) cluster states, which together represent only a small piece of the graph state needed to simulate a given quantum circuit. In this way, one minimizes the temporal accumulation of errors on qubits. This strategy also minimizes the vertex degree of any given vertex in the resulting graph states, which is advantageous for state purification protocols [35, 36]. These features come at a cost, however; the entanglement cannot be all generated before the computation begins as it is in the usual measurement-based model. This proposal therefore consists of a hybrid of 1WQC and the quantum circuit method. Second, each of the qubits in these small cluster states are in fact encoded qubits representing a five-qubit QECC, so that any single-qubit error that occurs on any of the (two or four) encoded qubits can be detected and corrected before any gate teleportation.

Computation proceeds by first encoding the left qubit(s) into the QECC, performing the encoded entangling gates with the right qubit(s), decoding the QECC on the left, making the syndrome measurements, and then performing the desired gate teleportation by measurement. After the gate teleportation from the left to the right, the logical cluster states are again re-built in two columns by re-encoding the previously measured qubits on the left, and entangling these with the logical state encoded on the five (or 10) physical qubits on the right. The procedure is repeated right-to-left, and then

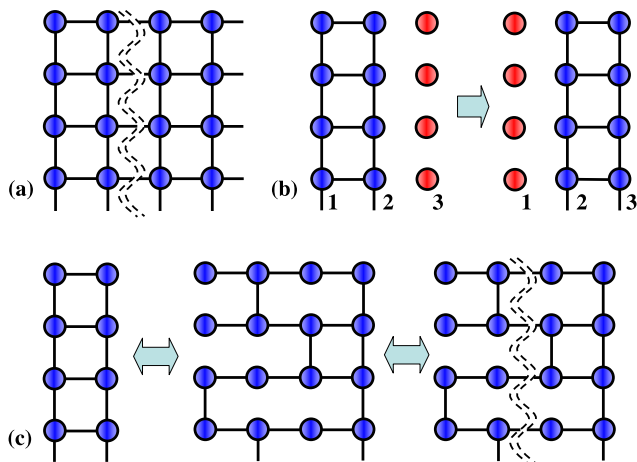


FIG. 1: (a) A regular 2D cluster state is comprised of qubits (shown as blue dots) entangled with their nearest neighbors (solid lines). Alternatively, it can be considered as a two-column cluster state, in which entangled qubits in column 2 are not yet entangled with qubits in column 3 (red dots), as shown in (b). Only after measurements on qubits in column 1 (subsequently shown in red) teleport gates to qubits in column 2, the qubits in columns 2 and 3 are entangled, and so on. In (c), the two-column cluster state is equivalent to a larger 2D cluster state, which in turn can be split into further two-column cluster states, shown on the right.

back again, until the entire computation is accomplished.

In many physical systems, the qubits are naturally arranged in a regular two-dimensional (2D) lattices, such as ultracold neutral atoms confined in optical lattices, quantum dots, or charge and flux superconducting qubits. These systems are often characterized by local single-qubit measurements, but global entangling gates, i.e. where each qubit becomes entangled with its nearest neighbors down a given axis. In principle, regular 2D cluster states, which are a universal resource for 1WQC [37, 38], can be readily formed dynamically in principle by applying simple spin Hamiltonians with quantum dots [39, 40, 41, 42, 43], superconducting qubits [44, 45, 46], and atoms in optical lattices [47, 48, 49]. Rather than a complication, global entangling gates can be harnessed in order to simultaneously encode the qubit(s) on one side while decoding the qubit(s) on the other. This efficient technique also allows for a dramatic reduction in the number of entangling operations required during the whole procedure.

A regular 2D cluster state is shown in Fig. 1(a). Qubits are initialized in the state  $|+\rangle = (|0\rangle + |1\rangle)/\sqrt{2}$ , which is the positive eigenvector of the Pauli- $X$  operator, and nearest-neighbor qubits are maximally entangled through the controlled-phase gate  $CZ = \text{diag}(1, 1, 1, -1)$ . In the usual approach to 1WQC, measurements are made on qubits column by column from left to right, which teleport gates in the same direction. Measurements are made in the Pauli- $XY$  plane spanned by the vectors  $|\pm_\xi\rangle = (|0\rangle \pm e^{i\xi}|1\rangle)/\sqrt{2}$  corresponding to the operator

$HR_z(\xi)$  where  $R_z(\xi) = \begin{pmatrix} e^{-i\xi/2} & 0 \\ 0 & e^{i\xi/2} \end{pmatrix}$  generates a rotation about the Pauli- $Z$  axis. On outcome  $m \in \{0, 1\}$ , the measurement has the effect of teleporting the gate  $X^m HR_z(\xi)$ , where  $H$  is the Hadamard operator. Three of these gates with different choices of  $\xi$  are sufficient to simulate a general single-qubit unitary. Together with the vertical  $CZ$  links that simulate entangling gates between logical qubits, 1WQC is able to simulate any quantum circuit, and is one of many approaches in the general measurement-based model of quantum computation [50].

Because of the linearity of the  $CZ$  gates, the computation on the full 2D cluster can be instead constructed as a sequence of teleportations and column-to-column entangling operations, as shown in Fig. 1(b). Qubits in the first two columns are first entangled, and a gate teleportation is effected by measurements of qubits in column 1. The qubits in the second column are only then entangled with those in column 3, and the procedure is repeated. Evidently, only two columns of qubits are ever actually needed in order to reproduce the full 2D cluster. The qubits in the left column are initially measured and the gate is teleported to qubits on the right; after re-entangling the two columns, measurement of qubits on the right will teleport another gate back to qubits on the left, etc. A similar idea has been recently discussed in Ref. [28, 51].

As illustrated in Fig. 1(c), the 2D cluster state can always be decomposed into a series of two-column graph states that are characterized by only two different kinds of subgraphs. These correspond to a two-qubit graph state  $|g_-\rangle \equiv CZ_{1,2}|+\rangle_{1,2}$  oriented horizontally, and the four-qubit linear cluster state in the ‘horseshoe’ shapes  $\square$  or  $\sqsupset$ ,  $|g_\square\rangle = |g_\sqsupset\rangle \equiv CZ_{1,2}CZ_{2,3}CZ_{3,4}|++++\rangle_{1,2,3,4}$ . This decomposition is always possible because inserting additional qubits along a horizontal axis simply requires additional measurements in the  $X$  basis, which teleport trivial (Clifford group) operators. Evidently, the same decomposition is also possible with computational cluster states, in which physical qubits are removed from the 2D cluster by computational basis (Pauli- $Z$ ) measurements. Thus, to effect universal quantum computation, one requires only multiple copies of the two states  $|g_-\rangle$  and  $|g_\square\rangle$ .

The remaining ingredient, and the core of the present work, is to encode each physical qubit in the states  $|g_-\rangle$  and  $|g_\square\rangle$  into QECC graph states. To minimize the overhead in terms of physical qubits, and the complexity of forming the states, we focus on the five-qubit QECC. A logical qubit  $A$  with five physical qubits (labeled 1 through 5) is represented by [4]

$$|0^L\rangle_A = \frac{1}{4}(|00000\rangle + |10010\rangle + |01001\rangle + |10100\rangle + |01010\rangle - |11011\rangle - |00110\rangle - |11000\rangle - |11101\rangle - |00011\rangle - |11110\rangle - |01111\rangle - |10001\rangle - |01100\rangle - |10111\rangle + |00101\rangle), \quad (1)$$

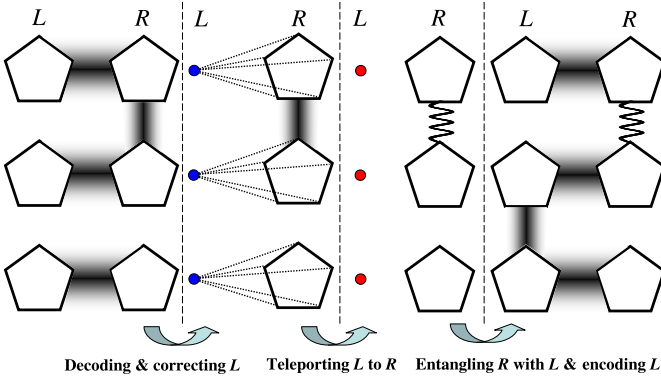


FIG. 2: A scheme for 1WQC is depicted in a two-column cluster state (pentagon; logical qubit and blurred line; logical  $CZ$  operation). One performs decoding on logical qubits and check error syndromes by measurement on ancillary physical qubits in column  $L$ . The error-corrected qubits are teleported to logical qubits in column  $R$  (red dot; measured physical qubit and wiggled line; preexisted  $CZ$  operation). Logical qubits are re-built in column  $L$  as long as logical  $CZ$  operations are performed among the logical qubits, and then it is ready to repeat all the procedure from the right to the left.

and the other logical qubit on site  $A$  is equal to

$$|1^L\rangle_A = X_A^L|0^L\rangle_A = X_{1-5}^{\otimes 5}|0^L\rangle_A, \quad (2)$$

where  $X_A^L$  and  $Z_A^L = Z_{1-5}^{\otimes 5}$  are logical Pauli- $X$  and  $Z$  operations on the logical qubit  $A$  and are fully transversal (see details in Ref. [52]). Then, the eigenvectors of  $X_A^L$ , hitherto referred to as logical Hadamard states, are also defined by

$$|\pm^L\rangle_A = (|0^L\rangle_A \pm |1^L\rangle_A)/\sqrt{2}. \quad (3)$$

These are equivalent to a pentagon graph state:

$$|^-^L\rangle_A \equiv |\diamond\rangle_A = C_{1-5}^{\diamond} |+\rangle_{1-5}^{\otimes 5}, \quad (4)$$

$$|^+^L\rangle_A \equiv |\tilde{\diamond}\rangle_A = Z^L |\diamond\rangle_A = C_{1-5}^{\tilde{\diamond}} |-\rangle_{1-5}^{\otimes 5}, \quad (5)$$

where  $|\pm\rangle_{1-5}^{\otimes 5} = |\pm\rangle_1|\pm\rangle_2|\pm\rangle_3|\pm\rangle_4|\pm\rangle_5$  and  $C_{1-5}^{\diamond} = CZ_{1,2}CZ_{2,3}CZ_{3,4}CZ_{4,5}CZ_{5,1}$ . If needed, the logical computational basis states can also be obtained directly from these via  $|1^L\rangle_A = X_A^L|0^L\rangle_A$  and

$$\begin{aligned} |0^L\rangle_A &= H_1 X_{2-5}^{\otimes 4} \prod_{m=3}^4 CZ_{1,m} CZ_{2,m} CZ_{5,m} |^-^L\rangle_A \\ &= H_1 X_{2-5}^{\otimes 4} CZ_{2,3} CZ_{2,5} CZ_{4,5} |K_5\rangle_A, \end{aligned} \quad (6)$$

neglecting an overall sign, where  $|K_5\rangle_A = \prod_{m=1}^4 \prod_{n=m+1}^5 CZ_{m,n} |+\rangle_{1-5}^{\otimes 5}$  is the complete graph on five qubits.

Fig. 2 shows a schematic for 1WQC in the two-column format ( $L$  and  $R$ ) discussed above, for a decomposed 2D cluster state. This particular example corresponds to the first two columns and first three rows of the third graphic

shown in Fig. 1(c). In the first step, logical cluster states are prepared in two columns. The pentagon shape denotes a logical qubit in the state  $|\pm^L\rangle$  (the choice of  $|\diamond\rangle$  or  $|\tilde{\diamond}\rangle$  is arbitrary because the  $Z^L$  and  $CZ$  gates commute). A blurred line represents a logical  $CZ$  operation (defined formally in the next Section). After decoding the logical qubits and performing syndrome measurements on four of the five qubits comprising each  $|\diamond\rangle$  on the left (second step), a teleportation scheme performed by single-qubit measurements on the fifth qubits in column  $L$  transfers the quantum information to the logical qubits in column  $R$  (third step in Fig. 2). Last, logical  $CZ$  operations are carried out to re-encode the physical qubits in column  $L$ , and to perform the various logical  $CZ$  operations according to the computational cluster being simulated. The full procedure is then repeated from right to left, and then back again, until the desired computation is done.

The proposed scheme is thus a hybrid of the 1WQC and quantum circuit models, combining the main advantages of both while minimizing the disadvantages. The main apparent advantage in the 1WQC model, that all of the entanglement can be generated in advance, is not in fact applicable when the probability of single-qubit errors is assumed to be constant with time: distant portions of the cluster state will be heavily distorted by the time measurements are made. By generating entanglement in only two columns at a time, this problem is mitigated. Meanwhile, the main advantage of standard 1WQC, that the nearest-neighbor entangling can be performed using a single global operation, is preserved in the current approach. Yet effective arbitrary two-qubit gates can still be performed, in the spirit of the circuit model. That said, some parallelism of the 1WQC model caused by the sequential error-checking stage is inevitable in the encoding and decoding procedures, but the total number of required operations is much smaller than it would be in the standard circuit model, as discussed in more detail below.

The remainder of this paper is organized as follows. In Sec. II, the mathematical formalism for the formation of QECC cluster states is described, and the procedure for implementing 1WQC is discussed. A practical approach to implementing these ideas for systems characterized by local single-qubit gates but global entangling operations is shown in Sec. III, and the results are analyzed in Sec. IV.

## II. THEORY OF 1WQC USING 5-QUBIT QECC

The full theoretical approach for 1WQC with embedded five-qubit quantum error correction can now be presented. The  $CZ$  operation can be represented as

$$CZ_{i,j} = \frac{1}{2} (I_i I_j + I_i Z_j + Z_i I_j - Z_i Z_j), \quad (7)$$

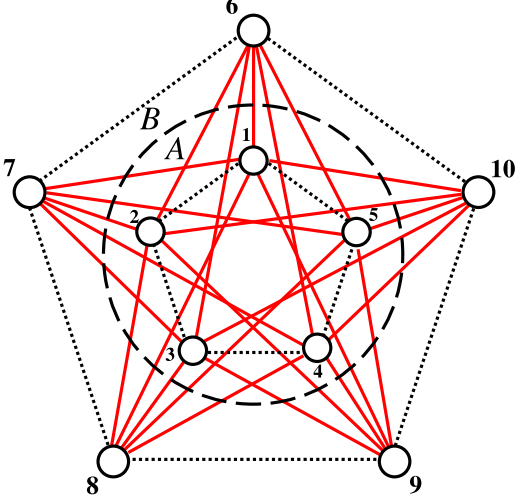


FIG. 3: A logical two-qubit cluster state  $|LCS_2\rangle_{AB}$  is depicted (see Eq. 13). Inner (outer)-pentagon qubits correspond to logical qubit  $A$  ( $B$ ) while the red lines indicate physical  $CZ$  operations between physical qubits.

so that a physical two-qubit cluster state between qubits 1 and 2 is equivalent to

$$CZ_{1,2}|+\rangle_1|+\rangle_2 = \frac{1}{\sqrt{2}}(|0\rangle_1|+\rangle_2 + |1\rangle_1|-\rangle_2). \quad (8)$$

Likewise, the logical  $CZ$  gate can be represented as

$$CZ_{A,B}^L = \frac{1}{2} (I_A^L I_B^L + I_A^L Z_B^L + Z_A^L I_B^L - Z_A^L Z_B^L), \quad (9)$$

where  $I_A^L = I_{1-5}^{\otimes 5}$ , so that the logical two-qubit cluster state is

$$CZ_{A,B}^L |^{-L}\rangle_A |^{-L}\rangle_B = \frac{1}{\sqrt{2}} (|0^L\rangle_A |^{-L}\rangle_B - |1^L\rangle_A |^L\rangle_B). \quad (10)$$

Of course, the logical  $CZ$  gate (9) is impossible to implement directly. Rather, one needs to know how to obtain the resulting state (10) using only two-qubit  $CZ$  gates and possibly local unitaries. To make further progress, it is useful to note that a six-qubit GHZ state can be constructed by adding a sixth qubit initialized in the  $|+\rangle$  state as follows:

$$\begin{aligned} |6GHZ\rangle_{1-5,6} &= \left[ \prod_{n=1}^5 CZ_{n,6} \right] |+\rangle_{1-5}^{\otimes 5} |+\rangle_6 \\ &= \frac{1}{\sqrt{2}} (|+\rangle_{1-5}^{\otimes 5} |0\rangle_6 + |-\rangle_{1-5}^{\otimes 5} |1\rangle_6). \end{aligned} \quad (11)$$

Applying the operation  $C_{1-5}^{\diamond}$  on the GHZ state, a logical-physical cluster state  $|\psi_{LP}\rangle$  is formed

$$\begin{aligned} |\psi_{LP}\rangle &\equiv C_{1-5}^{\diamond} |6GHZ\rangle_{A,6} \\ &= \frac{1}{\sqrt{2}} [ |^{-L}\rangle_A |0\rangle_6 + |^L\rangle_A |1\rangle_6 ], \end{aligned} \quad (12)$$

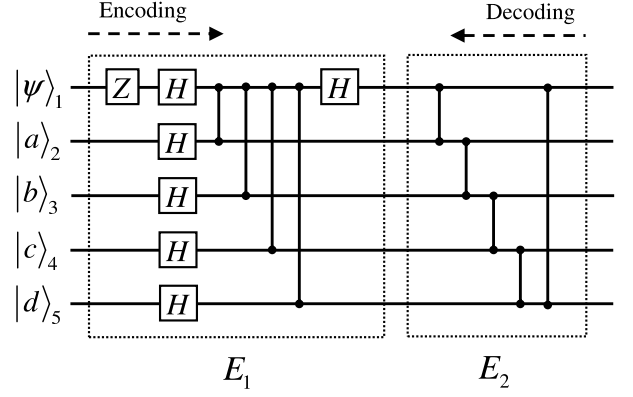


FIG. 4: For encoding  $|\psi\rangle_1 = \alpha|0\rangle_1 + \beta|1\rangle_1$  into a logical qubit, qubits 2 – 5 are prepared in  $|0000\rangle_{2345}$ . After operations  $E_1$  and  $E_2$ , the final state is  $\alpha|0^L\rangle_1 + \beta|1^L\rangle_1$ .

which is equivalent to the state (8) with the substitution  $|+\rangle \rightarrow |^{-L}\rangle$  as shown in Eq. (4). By a straightforward extension of the above arguments, one can readily obtain a logical two-qubit cluster state with 10 physical qubits:

$$\begin{aligned} |LCS_2\rangle &\equiv C_{1-5}^{\diamond} C_{6-10}^{\diamond} \prod_{m=1}^5 \prod_{n=6}^{10} CZ_{m,n} |+\rangle_{1-5}^{\otimes 5} |+\rangle_{6-10}^{\otimes 5} \\ &= \frac{1}{\sqrt{2}} [ |^{-L}\rangle_A |0^L\rangle_B + |^L\rangle_A |1^L\rangle_B ]. \end{aligned} \quad (13)$$

That this is equivalent to (10) can be seen by noting that  $\prod_{m=1}^5 \prod_{n=6}^{10} CZ_{m,n} |+\rangle_{1-5}^{\otimes 5} |+\rangle_{6-10}^{\otimes 5}$  yields

$$\frac{1}{2} [ (|+\rangle_A^{\otimes 5} + |-\rangle_A^{\otimes 5}) |+\rangle_B^{\otimes 5} + (|+\rangle_A^{\otimes 5} - |-\rangle_A^{\otimes 5}) |-\rangle_B^{\otimes 5} ],$$

which due to relations (4) and (5) transforms into (10) upon the application of the  $C_{1-5}^{\diamond} C_{6-10}^{\diamond}$  operators.

The encoded two-qubit cluster state is depicted in Fig. 3. To build this state, all physical operations are decomposed by two groups of  $CZ$  operations. Two logical qubits  $A$  (1 to 5) and  $B$  (6 to 10) are linked with five GHZ-type connections and two pentagon operations, and these  $CZ$  operations importantly commute with each other. The resulting ten-vertex graph has constant vertex degree seven. Likewise, the encoded version of the horseshoe subgraphs  $\square$  and  $\square$  are twenty-vertex graphs, with ten of the vertices (corresponding to encoded vertices at the two endpoints of the linear cluster state  $g_{\pm}^L$ ) having degree seven, and the remaining vertices (encoded vertices in the interior of the cluster state) having degree twelve.

### A. Encoding and decoding circuits

While  $C^{\diamond}$  is sufficient to effect the transformation  $|+\rangle^{\otimes 5} \rightarrow |^{-L}\rangle$ , after one gate teleportation the resulting state will instead be  $|\psi^L\rangle = \alpha|0^L\rangle + \beta|1^L\rangle$ , with  $\alpha, \beta$

arbitrary complex coefficients. Furthermore, under certain circumstances it may be desirable to initialize the 1WQC with some particular quantum state. The quantum circuit for encoding a physical qubit in the state  $|\psi\rangle_1 = \alpha|0\rangle + \beta|1\rangle$  into a logical qubit consisting of five physical qubits is shown in Fig. 4. The encoding consists of two sets of operations, labelled  $E_1$  and  $E_2$ . Suppose that five physical qubits are initially prepared in the state  $|\psi\rangle_1|0000\rangle_{2-5}$ . After  $E_1$ , one obtains the five-qubit state

$$|\tilde{\psi}\rangle_{1-5} = \frac{1}{\sqrt{2}} [(\alpha - \beta)|+\rangle_{1-5}^{\otimes 5} + (\alpha + \beta)|-\rangle_{1-5}^{\otimes 5}]. \quad (14)$$

The second circuit  $E_2$  maps vectors  $|\pm\rangle^{\otimes 5}$  into logical Hadamard states, as discussed in the previous section. Thus, the final state becomes

$$|\psi^L\rangle_{1-5} = C_{1-5}^\diamond |\tilde{\psi}\rangle_{1-5} = \alpha|0^L\rangle_{1-5} + \beta|1^L\rangle_{1-5}. \quad (15)$$

Evidently, for the special case  $|\psi\rangle_1 = |+\rangle_1$  where  $\alpha = \beta = 1/\sqrt{2}$ , one obtains  $E_2 E_1 |+\rangle_{1-5}^{\otimes 5} = |^L\rangle_{1-5} = Z^L C^\diamond |+\rangle_{1-5}^{\otimes 5}$ .

The decoding is simply the adjoint of the encoding circuit, as usual. For example, the detection outcome in  $|abcd\rangle_{2345}$  becomes  $|0000\rangle_{2345}$  without an error, because decoding is an inverse process of encoding qubits. Otherwise, the detected errors in  $|abcd\rangle_{2345}$  represent the physical qubit that suffered a Pauli error, and which type of error occurred (see the details in Table I). Thus, quantum error-correction is perfectly possible with corresponding syndrome measurements.

### B. Encoded teleportation

An encoded (or error-correcting) teleportation with two logical qubits is one of the main building blocks of encoded 1WQC. In Fig. 5, the first qubit  $|\psi\rangle_1$  has quantum information and nine physical qubits are initially

Error type	Syndrome ( $ abcd\rangle_{2345}$ )	Outcome
None	0000	
$Z_2$	1000	$ \psi\rangle$
$Z_3$	0100	
$Z_4$	0010	
$Z_5$	0001	
$X_1$	1001	
$X_3$	1010	$X \psi\rangle$
$X_4$	0101	
$X_3 Z_3$	1110	
$X_4 Z_4$	0111	
$X_1 Z_1$	0110	$XZ \psi\rangle$
$X_2$	1011	
$X_5$	1101	
$X_2 Z_2$	0011	
$X_5 Z_5$	1100	
$Z_1$	1111	$Z \psi\rangle$

TABLE I: Error correction table with corresponding syndrome detections in the decoder circuit in Fig. 4.

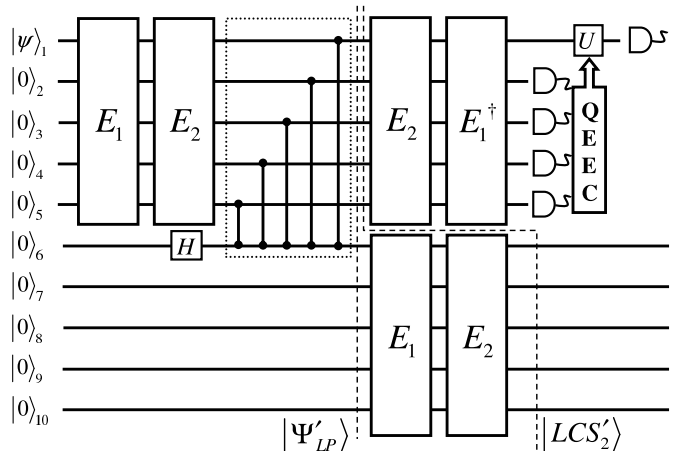


FIG. 5: The full quantum circuit is shown for encoded teleportation between the first encoded qubit (physical qubits 1 – 5) and the second (qubits 6 – 10). Encoding is accomplished by the unitaries  $E_1$  and  $E_2$  shown in Fig. 4. The two logical encoded qubits are then entangled by a GHZ-type interaction between the first five physical qubits and qubit 6. The first logical qubit is decoded via  $E_2^\dagger$  and  $E_1^\dagger$ , syndrome measurements on qubits 2 – 5 are performed, and teleportation is finally accomplished via measurement of qubit 1.

prepared in the state  $|0\rangle$ . The encoding operations ( $E_1$  and  $E_2$ ) on the first five qubits then yield logical qubit  $A$ . Alternatively, the first five qubits would represent a logical state  $|\psi^L\rangle_{1-5}$  that was the result of some previous, in which case one would ignore the  $E_2 E_1$  operation. In the middle of Fig. 5, a GHZ operation  $\prod_{n=1}^5 CZ_{n,6}$  including a Hadamard operation in qubit 6 creates the logical-physical cluster state

$$|\psi'_{LP}\rangle = \alpha|0^L\rangle_{1-5}|+\rangle_6 + \beta|1^L\rangle_{1-5}|-\rangle_6. \quad (16)$$

The subsequent encoding of logical qubit  $B$  yields the desired final state

$$|LCS'_2\rangle_{AB} = \alpha|0^L\rangle_A|^L\rangle_B + \beta|1^L\rangle_A|^{-L}\rangle_B. \quad (17)$$

Note that the quantum circuit shown in Ref. 5 requires only the single GHZ operation  $\prod_{n=1}^5 CZ_{n,6}$ . This is in apparent contrast with the logical two-qubit state depicted in Fig. 3. In fact, if one were to ‘push’ the  $E_1$  and  $E_2$  operations on qubits 6-10 through this GHZ operation, one would indeed recover the implied graph-state connections. More precisely, it is straightforward to verify that

$$\begin{aligned} & E_2 E_1 \prod_{n=1}^5 CZ_{n,6} H_6 |0\rangle_{6-10}^{\otimes 5} \\ &= Z_{6-10}^L C_{6-10}^\diamond \prod_{n=1}^5 \prod_{m=6}^{10} CZ_{n,m} |+\rangle_{6-10}^{\otimes 5}. \end{aligned} \quad (18)$$

It is clearly preferable in practice to implement the quantum circuit shown in Fig. 5 than to explicitly perform all

of the GHZ operations on the right-hand side of Eq. (18).

Now, quantum information is protected from a single-Pauli error in the logical two-qubit cluster state. After decoding and measuring syndromes in logical qubit  $A$ , the error can be corrected in qubit 1, yielding the intermediate physical-logical state

$$|\psi_{PL}\rangle_{1,B} = \alpha|0\rangle_1|+^L\rangle_B + \beta|1\rangle_1|-^L\rangle_B. \quad (19)$$

It is easy to check that a measurement of the first qubit in the  $HR_z(\xi)$  basis with outcome  $m \in \{0, 1\}$  yields the result

$$\begin{aligned} |\psi_{\text{out}}^L\rangle &= \frac{e^{-i\xi/2}}{\sqrt{2}} [(\alpha \pm e^{i\xi}\beta) |0^L\rangle_B + (\alpha \mp e^{i\xi}\beta) |1^L\rangle_B] \\ &= (X^L)^m H^L R_z^L(\xi) |\psi^L\rangle_B, \end{aligned} \quad (20)$$

which yields precisely the desired gate on the encoded qubit  $B$  required to construct a universal unitary operation on the logical state. The generalization of the above results to the encoded horseshoe subgraph is straightforward.

### III. PHYSICAL IMPLEMENTATION

Even with the simplified quantum circuit for encoding the two-qubit cluster state shown in Fig. 5, compared with the full graph state shown in Fig. 3, there remain 23 physical two-qubit gates in order to implement the logical two-qubit cluster state. The situation with the encoded linear four-qubit states is worse yet, with 51 physical two-qubit gates. The number of such operations can be greatly reduced, however, in physical systems characterized by global entanglement operations, such as quantum dots [39, 40, 41, 42, 43], superconducting qubits [44, 45, 46], and atoms in optical lattices [47, 48, 49].

Several proposals for the generation of cluster states using global interactions have been theoretically studied in solid-state systems. A single quantum-dot qubit consists of two charge states in a double-well potential coupled to a long transmission resonator [41]. Two electrons can be located in either the left or right potential well. When the double-well is biased by an external field, the charge states can be encoded as computational qubit states. The application of an oscillating field to each qubit then yields a linear cluster state [41, 42], or an encoded cluster state with multiple dots [43]. Similarly, a superconducting qubit consists of Josephson junctions connected to a common inductance. For example, a superconductor ring consisting of three Josephson junctions can provide a phase qubit in a double-well potential in which circulating supercurrents of opposite circulation are computational states. By turning on the inter-qubit inductive coupling, a linear cluster state can be created in the superconductor array [44, 45, 46].

As the other concrete example discussed in the remainder of this work, consider ultracold atoms confined

in 2D optical lattices. Ideally in the Mott-insulator state [53, 54, 55], exactly one atom will occupy each site of a 2D lattice. The Mott limit has been achieved for arbitrary dimensions [56], though in the 1D and 2D cases it is difficult to reach the regime of unit filling [57, 58, 59]. Entanglement between each nearest-neighbor can then be effected across the system using either state-dependent collisions [49, 53] or tunable spin-spin interactions [47]. In both cases, the entanglement operation is global, i.e. is effected between all neighbors simultaneously along a given direction. Errors in the application of the global entangling gate will generally result in a two-qubit controlled-phase gate  $\text{diag}(1, 1, 1, e^{i\phi})$  with  $\phi \neq \pi$ , which would have serious consequences for the application of 1WQC in these systems. A global phase error can be eliminated in principle [60], but random phase errors are more difficult to correct [61].

Only using state-dependent collisions, however, can the choice of neighbors be easily controlled by suitable time-dependent manipulation of the lattice potential in both spatial directions. In order to apply this idea to our QECC scheme, every five qubits should be encoded as a logical qubit in optical lattices. In particular, construction of all encoded two- or four-qubit cluster states in a given column of the full computational cluster requires at most five entangling operations. Furthermore, the decoding circuit  $E_1^\dagger E_2$  on the first logical qubit, shown in Fig. 5, can be performed simultaneously with the encoding circuit  $E_2 E_1$  on the second qubit. Thus, each gate teleportation for all logical qubits requires a total of five entangling gates.

The actual implementation of 1WQC still remains experimentally challenging because the distance between adjacent lattice sites is usually comparable to the spatial size of the laser beam used for single-qubit operations. This means that applying single-qubit rotation might yield undesirable operations on neighboring atoms of the target atom using a single laser field. Several proposals for improving the addressability have recently been made. For example, interference of laser beams allows single-qubit operations with many-atom addressing [62]; other proposals include employing microwave transitions [63] or pointer atoms [64]. Much experimental progress has been made toward single-atom addressing [65]. One approach is to make a larger separation between the neighboring atoms. A superlattice scheme using lasers at two different wavelengths enables loading of atoms at every third site of the optical lattice [66]. More recently, images of single atoms in 3D optical lattices can be taken either through the use of a high-resolution lens [67] or lattices with large spacing [68]. Alternatively, atoms loaded into optical lattices [69] can be rearranged by using two crossed beams [70] to end up in regions more amenable to addressing.

In this section, we show how to generate logical two-qubit and four-qubit cluster states in such a system. The main idea is to use auxiliary physical qubits (ancillae) in the vicinity of the qubits comprising the logical states, in



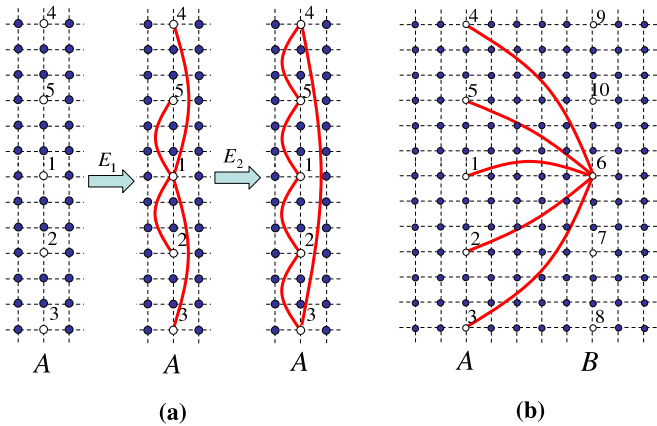


FIG. 6: An overview of the procedure for producing the logical-physical cluster state in a regular lattice is shown. The encoding operation on the five physical qubits (white dots aligned in a single column) of logical qubit  $A$  is shown in (a). Blue dots denote auxiliary qubits which mediate a  $CZ$  operation (red line) between two distant qubits. Pauli- $Z$  and Hadamard operations are first performed on the information qubit  $|\psi\rangle_1$  (see Fig. 4), while the other four relevant qubits (2-5) and the remaining unneeded physical qubits are initially prepared in the computational basis state  $|0\rangle$ . The approach for obtaining the operations  $E_1$  and  $E_2$  are shown in Figs. 7 and 8, respectively. The distant GHZ operation depicted in (b) between qubits 1-5 and qubit 6 is shown in Fig. 9. When we perform all the operations in (a) and (b) including several single-qubit operations shown in Fig. 4, the final state is  $|\psi'_{LP}\rangle_{AB}$  in Eq. (16).

order to effect entanglement between two spatially distant physical qubits. We also illustrate that encoding and decoding can be performed simultaneously on different logical qubits using global  $CZ$  operations, allowing for a significant reduction in the number of overall operations. Finally, we suggest various strategies for approaching fault-tolerance in these systems.

### A. Two-qubit encoded cluster states

The quantum circuit for the encoded teleportation is shown in Fig. 5, but this cannot be directly implemented in systems characterized by global entangling operations because it requires entanglement gates between distant qubits. An appropriate strategy for producing a logical-physical cluster state in a 2D square system is shown in Fig. 6. All of the sites colored blue are qubits that serve as ancillae, and are initialized in  $|0\rangle$ ; the white dots are physical qubits comprising logical qubits  $A$  and  $B$ , labeled from 1 to 5 and 6 to 10 in Fig. 6, respectively. The encoding of qubits in  $A$  requires single-qubit operations on the physical qubits, and two graph circuits: the  $\text{GHZ}_5$  and the pentagon operator  $C_{1-5}^{\diamond}$ , both shown in Fig. 4. As shown below, these can each be performed independently with two global entangling gates (in the ver-

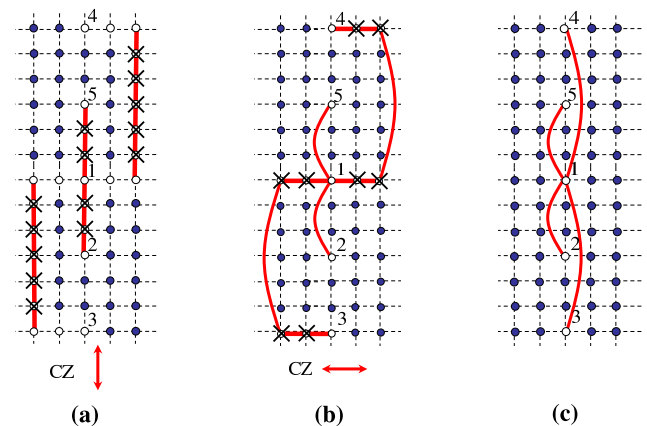


FIG. 7: Two global entangling operations are required to build the  $E_1$  circuit. (a) Blue and white dots are initialized in states  $|0\rangle$  and  $|+\rangle$ , respectively. After a vertical global  $CZ$  operation (red lines), various qubits are measured in the  $X$  basis (denoted by the  $\times$  symbol). (b) After a horizontal global  $CZ$  operation and further measurements, one obtains the desired outcome (c).

tical and horizontal directions) using the nearby ancillary qubits. The logical-physical cluster state is finally formed with the  $\text{GHZ}_6$  operator  $\prod_{i=1}^5 CZ_{i,6}$  shown in Fig. 6(b), and implemented explicitly below using three global entangling operations. The logical-physical cluster state can therefore be obtained using a total of seven global entangling operations.

The implementation of the four entangling operations in the  $E_1$  circuit is depicted in Fig. 7. All of the qubits are initialized either in the states  $|0\rangle$  (blue) or  $|+\rangle$  (white). A single global entangling operation is then performed in the vertical direction, which results in  $CZ$  gates between each pair of white qubits (shown as straight red lines in the figure). Measurements in the  $X$  basis (depicted as crosses in the figure) are then performed on selected ancillae in order to produce a  $CZ$  gate between distant qubits (shown as curved red lines in the figure). Because each measurement teleports an  $X^m H$  gate to the neighboring qubit, where  $m = \{0, 1\}$  denotes the measurement outcome, one must measure an even number of qubits between each pair. Alternatively, one could choose to measure an odd number of intervening qubits, but then a Hadamard gate would have to be applied manually to any qubit at the end of the distant  $CZ$  bond. This latter approach would require fewer ancillae, but unnecessarily complicates the present discussion. A subsequent entangling operation in the horizontal direction, followed again by an even number of  $X$  measurements and the application of appropriate single-qubit gates, results in the four  $\text{GHZ}_5$  entangling operations needed for the  $E_1$  circuit.

The five entangling gates  $C_{1-5}^{\diamond}$  in the circuit  $E_2$  can be implemented in an analogous fashion, as shown in Fig. 8. The qubits are initialized in either  $|0\rangle$  or  $|+\rangle$ , a global vertical entangling operation is performed, fol-

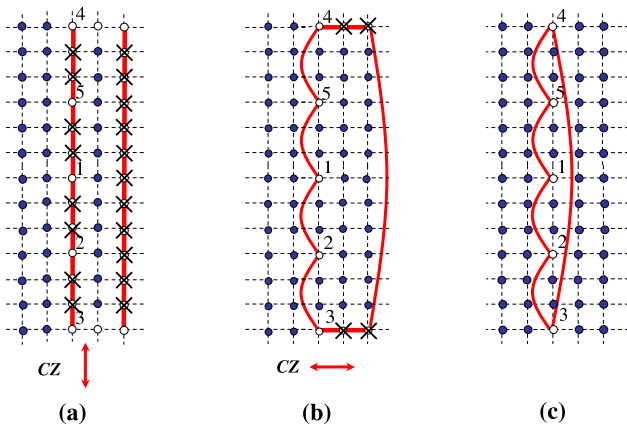


FIG. 8: Two global entangling operations are also required to build the  $E_2$  circuit. (a) Blue and white dots are initialized in states  $|0\rangle$  and  $|+\rangle$ , respectively. After a vertical global  $CZ$  operation (red lines), various qubits are measured in the  $X$  basis (denoted by the  $\times$  symbol). (b) After a horizontal global  $CZ$  operation and further measurements, one obtains the desired outcome (c).

lowed by various measurements and single-qubit gates to compensate for byproduct operators associated with measurement outcomes  $m = 1$ . A subsequent horizontal global entanglement operation and further measurements yields the desired gate set. Note that for the last set of measurements, one cannot naively apply single-qubit  $X$  gates to compensate for byproduct operators, because these do not commute with the  $CZ$  operators; rather, the byproduct operators must be kept in mind during the usual feed-forward process of the one-way computation.

The final task is to create the  $\text{GHZ}_{1-5,6}$  operation between each of five qubits of the logical qubit  $A$  and physical qubit 6,  $\prod_{n=1}^5 CZ_{n,6}$ . While the approach is again similar to the methods described above to generate entanglement between remote qubits in circuits  $E_1$  and  $E_2$ , in the present case one rather requires three global entangling gates. This might at first seem surprising, because one requires a set of entangling gates that is almost identical to those needed for  $E_1$ . The reason is that qubit 6 needs to be entangled with five other qubits, whereas in  $E_1$  qubit needed to entangle with only four other qubits. With a square lattice geometry where each qubit has four neighbors, entangling a central qubit to four other qubits is straightforward, but not to five.

The scheme for implementing the  $\text{GHZ}_{1-5,6}$  operations in the lattice is shown in Fig. 9. After suitable initialization of qubits, a horizontal global entangling gate is applied. After suitable measurements and applied single-qubit unitaries, a vertical global entangling gate is applied. Again making measurements and applying unitaries, one obtains entanglement between qubit 6 and qubits 1, 2, and 5. In order to generate entanglement between qubit 6 and qubits 3 and 4, one requires one more

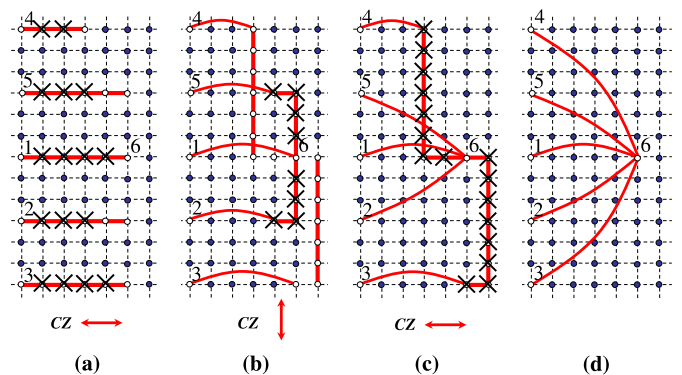


FIG. 9: Three global entangling operations are required to generate the  $\text{GHZ}_6$  entangling gates shown in Fig. 5. (a) Blue and white dots are initialized in states  $|0\rangle$  and  $|+\rangle$ , respectively. After a horizontal global  $CZ$  operation (red lines), various qubits are measured in the  $X$  basis (denoted by the  $\times$  symbol). (b) After re-initialization of various qubits a vertical global entangling gate is performed, and various measurements are made. (c) A subsequent re-initialization, vertical entangling operation, and set of measurements yields the desired outcome (d).

vertical global entangling operation and further measurements/unitaries.

With the approaches discussed above, one requires a total of seven global entangling operations, in addition to single-qubit measurements and unitaries, in order to produce the logical-physical cluster state  $|\psi'_{LP}\rangle$ . The full quantum teleportation circuit shown in Fig. 5 also requires the decoding of logical qubit  $A$  and the encoding of logical qubit  $B$ , followed by error-syndrome and gate-teleportation measurements. Once the information has been teleported, it will be encoded in logical qubit  $B$ , because the encoding operation  $E_2E_1$  will already have been carried out. The information and a logical gate can then be teleported back to  $A$  by replacing the indices 1–5 with 6–10, etc. Thus, each subsequent teleportation requires decoding  $B$  ( $A$ ), encoding  $A$  ( $B$ ), and performing the  $\text{GHZ}_{6-10,1}$  ( $\text{GHZ}_{1-5,6}$ ) entangling gates.

One nice feature of this proposal is that the decoding of  $A$  ( $B$ ) can be performed simultaneously with the encoding of  $B$  ( $A$ ). Both  $E_1$  and  $E_2$  are effected by a horizontal global entangling gate followed by a vertical one. Furthermore, the qubits in  $A$  and the ancillae used to mediate the distant  $CZ$  gates among them are well-separated from their counterparts in  $B$ . Thus, each encoded gate teleportation requires a total of seven global entangling operations. The only difference to Figs. 7-9 is that physical qubits comprising  $A$  ( $B$ ) are not re-initialized if the quantum information is encoded in logical qubit  $A$  ( $B$ ).

## B. Four-qubit encoded cluster states

To build the horseshoe graphs  $\square$  and  $\sqsupset$  of the computational cluster state, we need to perform only a distant



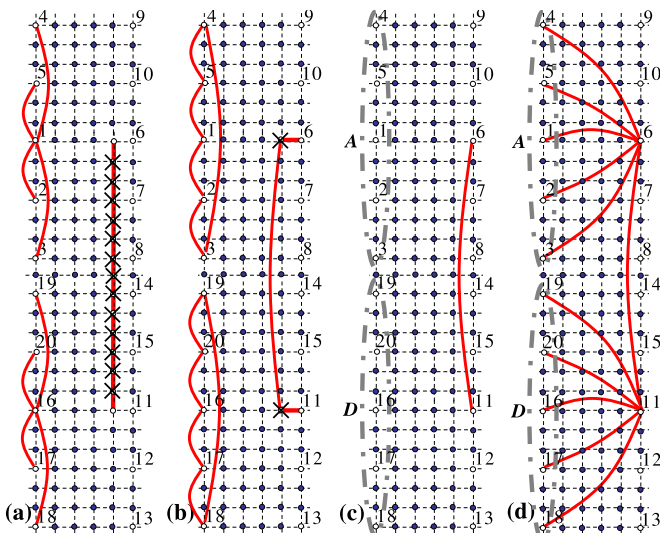


FIG. 10: Two logical qubits are denoted as  $A$  (qubits 1 to 5) and  $D$  (16 to 20). (a) During operation  $E_1$  in qubit  $A$  and  $D$ , a vertical global CZ operation is simultaneously created on the right side, and the middle qubits are measured in the  $X$  basis. (b) During operation  $E_2$  in qubit  $A$  and  $D$ , a horizontal global CZ operation is performed, and two auxiliary qubits are measured in  $X$  basis. (c) While logical qubits are successfully made in  $A$  and  $D$  (see the grey dot-dash ovals), a distant CZ operation is created between qubits 6 and 11. (d) Performing  $\text{GHZ}_6$  operation between logical qubit  $A$  and 6 ( $D$  and 11), a logical-physical four-qubit cluster state is created.

$CZ$  operation between the central qubit of a logical qubit and that of the other logical qubit. As shown in Fig. 10, four logical qubits are denoted as  $A$  (qubits 6 to 10),  $B$  (qubits 11 to 15), and  $D$  (16 to 20). Their central information qubit are called qubit 1, 6, 11, and 16, and prepared in states  $|\psi\rangle_1 = \alpha|0\rangle_1 + \beta|1\rangle_1$ ,  $|+\rangle_6$ ,  $|+\rangle_{11}$ ,  $|\phi\rangle_{16} = c|0\rangle_{16} + d|1\rangle_{16}$ , respectively. In Fig. 10(a), a vertical global CZ operation (a red straight line) is created, and the middle qubits are measured in the  $X$  basis (denoted by  $\times$  symbol) during operation  $E_1$  on qubits  $A$  (1 to 5) and  $D$  (16 to 20). Similarly, during operation  $E_2$  on qubits  $A$  and  $D$ , a horizontal global CZ operation is made between qubit 6 (11) and the auxiliary qubit and the two extra qubits are measured in  $X$  basis as shown in Fig. 10(b). Then, in Fig. 10(c), two logical qubits ( $A$  and  $D$ ) are built (see the grey dot-dash lines) while a physical two-qubit cluster state is made between qubits 6 and 11. This state yields

$$\frac{1}{\sqrt{2}} [|\psi^L\rangle_A (|0\rangle_6 |+\rangle_{11} + |1\rangle_6 |-\rangle_{11}) |\phi^L\rangle_D]. \quad (21)$$

In Fig. 10(d), the state becomes a logical-physical four-qubit cluster state with quantum information  $|\psi^L\rangle$  and  $|\phi^L\rangle$  after the  $\text{GHZ}_6$  operation between logical qubit  $A$  and physical qubit 6 ( $D$  and 11). Finally, when encoding  $E_2 E_1$  is performed in qubits  $B$  and  $C$ , the final state yields  $CZ_{AB}^L CZ_{BC}^L CZ_{CD}^L |\psi^L\rangle_A |+\rangle_B |+\rangle_C |\phi^L\rangle_D$

as the logical horseshoe graph  $\square$ .

### C. Toward fault tolerant 1WQC

The approach to one-way quantum computation described above has several advantages over the standard cluster-state model. First, the two-column approach means that physical qubits are prepared quickly and then immediately used. In this way, the accumulation of errors on resource qubits is minimized. Second, the quantum information is protected during a portion of the protocol, using the smallest possible QECC and the smallest number of entangling operations. In this way, single qubit errors are detected and corrected before they can be propagated by quantum teleportation. Third, in many physical implementations most of the entanglement gates required can be parallelized (for example, the encoding of multiple logical qubits can be performed simultaneously with the decoding of others), significantly lowering the number of required operations.

These advantages notwithstanding, the procedure is only weakly tolerant of single-qubit depolarizing errors. The information is only protected during the small temporal window immediately following the gate teleportation. That said, there are several small changes to the above protocol that would provide significant improvements to the protection of the quantum information, and furthermore point the way toward developing a fault-tolerant 1WQC protocol with suitably modified cluster states.

The first modification is to redesign the sequence of operations in order to protect the quantum information from single-qubit errors most of the time. In the current approach (see Fig. 5), the logical qubit  $A$  of a logical-physical two-qubit cluster state, Eq. (16), is decoded at the same time as logical qubit  $B$  is encoded. This has the advantage of minimizing the total number of entangling operations needed in systems where these can be performed in parallel. The disadvantage is that the quantum information residing on qubit  $A$  is susceptible to error during this process, as it is during the syndrome measurements, possible attendant single-qubit unitaries, and the gate teleportation measurement. It would be preferable if most if not all of these operations could all be performed on encoded information; and furthermore that they would be carried out fault-tolerantly.

To improve this scenario, qubit  $B$  could be encoded independently while the quantum information continues to reside in  $A$ , which in systems characterized by global entangling operations requires a total of four global entangling gates, as shown in Figs. 7 and 8. This approach has the definite advantage that the integrity of the encoding can be verified before the quantum information in  $A$  is teleported to  $B$ . As in the original protocol [8], one needs to construct a four-qubit GHZ state proximal to the logical state being tested; then four of the physical qubits comprising the logical state are each entangled

with one qubit of the GHZ state, followed by syndrome measurements on the GHZ qubits. The process is repeated four times to verify the logical state. Any error discovered can be repaired by performing the appropriate single-qubit operation on the logical state. Assuming perfect GHZ states (more on this below), the procedure is fault-tolerant, because of the relationship between the QECC stabilizer and the entangling operations between the logical and GHZ states. The full procedure should be performed several times in order to have confidence that the error syndrome is properly diagnosed.

Unfortunately, encoding qubit B before entangling with A modifies Fig. 5, in that the unitary  $E_2E_1$  is applied to qubits 6-10 *before* the  $\text{GHZ}_{1-5,6}$  operation. It is not difficult to show that this means that the full  $\text{GHZ}_{1-5,6-10}$  set of twenty five entangling gates depicted in Fig. 3 would instead need to be applied on the physical qubits. This is the main apparent drawback of employing the five-qubit QECC: because it is not a CSS code, a transversal  $CZ$  operation (i.e. a direct logical  $CZ$  gate between encoded qubits) is not possible. While the logical entangling gate cannot be applied fully fault-tolerantly without a large overhead in terms of ancillary qubits and operations, certain steps can nevertheless be verified.

The required set of gates can be simplified by noting that the graph state  $|g\rangle \equiv \prod_{i=1}^5 \prod_{j=6}^{10} CZ_{i,j}|+\rangle^{\otimes 10}$  is unitary equivalent to the graph state  $|g'\rangle \equiv CZ_{1,6} \prod_{i=2}^5 CZ_{1,i} \prod_{j=7}^{10} CZ_{6,j}|+\rangle^{\otimes 10}$  by edge complementation [71] (in this case between qubits 1 and 6). That is, one rather needs to first generate GHZ states on qubits 1-5 and 6-10, and then entangle together only one qubit from each set, for a total of only nine entangling gates. The edge-complementation equivalence does not apply directly to the qubits A and B, however, because one of these is an encoded state possessing the relevant quantum information, and is not the simple product state  $|+\rangle^{\otimes 5}$  assumed above.

One would rather insert ancillary qubits (labeled  $1'$  through  $5'$ ) just to the right of logical qubit A, oriented vertically and aligned horizontally with qubits 1 through 5; a similar set would be inserted to the left of logical qubit B (labeled  $6'$  through  $10'$ ). GHZ states  $|5\text{GHZ}\rangle_{1'-5'}$  and  $|5\text{GHZ}\rangle_{6'-10'}$  are prepared using the procedure shown in Fig. 7. The two GHZ states can then be entangled with each other using a single horizontal entangling operation and two additional ancillae, and the state depicted in Fig. 3 can be obtained by local operations. Logical qubits A and B are then entangled by applying a single horizontal global entangling gate, which entangles all qubit pairs  $i$  and  $i'$ ,  $1 \leq i, i' \leq 5$  through intermediate ancillae, followed by X measurements of qubits  $i$ .

The four and five-qubit GHZ states that are required to fault-tolerantly verify the encoded single qubit state and to mediate the logical qubit-qubit entangling operation, respectively, must themselves be verified prior to their use. In practise, one simple requires one additional phys-

ical qubit, which is repeatedly entangled with the GHZ state and then measured. If the measurement outcome indicates an error, the procedure is repeated. The ancilla would be a physical qubit directly above the GHZ qubits, so only one vertical entangling operation is needed for each verification measurement. A similar approach was recently proposed in ion traps [72].

All logical states and ancillary GHZ states can be verified fault-tolerantly after their (non fault-tolerant) construction. Thus, all operations in the 1WQC scheme discussed above can in principle be performed fault-tolerantly, except for the single entangling operation that links the ancillary five-qubit GHZ states to the logical qubits and to each other. This can be performed using fault-tolerant constructions, but is not in itself fault-tolerant because the fidelity of the result cannot be tested. In principle, this operation also could be made fault-tolerant through the use of additional ancillae and verification, but at the cost of completely repeating the construction of the logical qubit not encoding the quantum information. In practise, it is reasonable to assume that the time taken to perform these entanglement operations, during which the quantum information would be entangled fault-tolerantly but unverifiably, would be small compared to the time needed to perform the other operations.

#### IV. SUMMARY AND REMARKS

An approach to 1WQC has been presented that explicitly incorporates quantum error correction as a way to minimize the propagation of errors during the computational process. This proposal has two key features. First, the cluster states are only constructed two columns at a time, so that physical qubits will not have a sufficient amount of time to undergo significant decoherence prior to measurement. Second, QECC states are prepared in each column, where a logical qubit is equivalent to a five-qubit graph state, and a logical two-qubit cluster state is represented by a graph state of ten qubits. In this way, errors can be detected and corrected prior to the main gate teleportation. Each teleportation requires several procedures on the two logical qubits, including encoding, decoding,  $\text{GHZ}_6$  quantum circuits. Prior to the encoded teleportation, the error syndrome is checked by single-qubit measurements on four of the five physical qubits comprising the first logical qubit, and the corrected information is teleported to the next logical qubit.

Following the description of the fundamental protocol, a physical implementation is discussed for systems characterized by global entangling operations, such as ultracold atomic gases in 2D optical lattices. A procedure for constructing logical cluster states (logical two-qubit and four-qubit states) using several global  $CZ$  operations and single-qubit measurements is shown explicitly, with an eye on minimizing the number of physical (ancillary) qubits and total operations.

While the main scheme for error-correcting 1WQC discussed in the manuscript allows for error detection and correction, it is not fault-tolerant. An improved scheme is outlined that begins to address this issue, at the cost of additional ancillae and operations. This improved scheme incorporates fault-tolerant elements, but only hints at a fully fault-tolerant approach to one-way quantum computation based on quantum error correction. For example, the logical states are constructed using unprotected single-qubit and entangling gates, logical qubits are entangled by non-transversal and unverifiable operations, and concatenating the logical qubits in systems characterized by global entangling operations seems daunting.

In the circuit model, a concatenation method for five-qubit QECC has been already mathematically studied [73]. In our scheme, the first level of concatenation costs 25 physical qubits (five pentagon qubits) and 50 physical  $CZ$  operations among them using edge-complementation equivalence. Because of the mathematical complexity of the logical  $CZ$  operation in the first level concatenation, let alone determining how one would go about implementing it with physical qubits in

periodic lattices, a full investigation into how to implement concatenation with this approach is beyond the scope of the present work. Another fruitful extension of our work, concatenating two different QECCs and using larger codes to correct more noisy models, will also be needed in order to develop a more complete theory of practical fault-tolerant 1WQC. These issues, and a full analysis of the associated error thresholds, will be addressed in future work.

### Acknowledgments

The authors acknowledge fruitful conversations with Travil Beals. J.J. acknowledges iCORE and the Natural Sciences and Engineering Research Council of Canada. This work was supported by the Natural Sciences and Engineering Research Council of Canada, the Alberta Informatics Circle of Research Excellence, and the Mathematics of Information Technology and Complex Systems' Quantum Information Processing project.

- 
- [1] P. W. Shor, Phys. Rev. A **52**, 2493 (1995).
  - [2] A. R. Calderbank and P. W. Shor, Phys. Rev. A **54**, 1098, (1996).
  - [3] D. Gottesman, Phys. Rev. A **54**, 1862 (1996).
  - [4] C. H. Bennett, D. P. DiVincenzo, J. A. Smolin, and W. K. Wootters, Phys. Rev. A **54**, 3824 (1996).
  - [5] A. R. Calderbank, E. M. Rains, P. W. Shor, and N. J. A. Sloane, Phys. Rev. Lett. **78**, 405 (1997).
  - [6] E. Knill and R. Laflamme, Phys. Rev. A **55**, 900 (1997).
  - [7] R. Laflamme, C. Miquel, J. P. Paz, and W. H. Zurek, Phys. Rev. Lett. **77**, 198 (1996).
  - [8] D. P. DiVincenzo and P. W. Shor, Phys. Rev. Lett. **77**, 3260 (1996).
  - [9] E. Knill and R. Laflamme, R. Martinez, and C. Negrevergne, Phys. Rev. Lett. **86**, 5811 (2001).
  - [10] E. Knill, Phys. Rev. A **71**, 042322 (2005).
  - [11] E. Knill, Nature **434**, 39 (2005).
  - [12] E. Knill, R. Laflamme, W. Zurek, Science **279**, 342 (1998).
  - [13] A. M. Steane, Phys. Rev. A **68**, 042322 (2003).
  - [14] E. Knill and R. Laflamme, quant-ph/9608012 (1996).
  - [15] P. Aliferis, D. Gottesman, and J. Preskill, Quant. Inf. Comput. **6**, 97 (2006).
  - [16] A. Kitaev, Ann. Phys. **303**, 2 (2003).
  - [17] J. Preskill, quant-ph/9712048 (1997).
  - [18] J. Benhelm, G. Kirchmair, C. F. Roos, and R. Blatt, Nature Phys. **4**, 463 (2008).
  - [19] H. J. Briegel and R. Raussendorf, Phys. Rev. Lett. **86**, 910 (2001).
  - [20] R. Raussendorf, D. E. Browne, and H. J. Briegel, Phys. Rev. A **68**, 022312 (2003).
  - [21] H. J. Briegel, T. Calarco, D. Jaksch, J. I. Cirac, and P. Zoller, J. Mod. Opt. **47**, 415 (2000).
  - [22] M. A. Nielsen and C. M. Dawson, Phys. Rev. A **71**, 042323 (2005).
  - [23] P. Aliferis and D. W. Leung, Phys. Rev. A **73**, 032308 (2006).
  - [24] I. L. Chuang and Y. Yamamoto, Phys. Rev. Lett. **76**, 4281 (1996).
  - [25] M. S. Tame, M. Paternostro, and M. S. Kim, New J. Phys. **9**, 201 (2007).
  - [26] L. Jiang, A. M. Rey, O. Romero-Isart, J. J. Garcia-Ripoll, A. Sanpera, and M. D. Lukin, Phys. Rev. A **79**, 022309 (2009).
  - [27] R. Raussendorf, J. Harrington, and K. Goyal, Ann. Phys. **321**, 2242 (2006).
  - [28] R. Raussendorf and J. Harrington, Phys. Rev. Lett. **98**, 190504 (2007).
  - [29] R. Raussendorf, J. Harrington, and K. Goyal, New J. Phys. **9**, 199 (2007).
  - [30] R. Stock and D. F. James, Phys. Rev. Lett. **102**, 170501 (2009).
  - [31] S. J. Devitt, A. G. Fowler, A. M. Stephens, A. D. Green-tree, L. C. L. Hollenberg, W. J. Munro, K. Nemoto, arXiv:0808.1782 (2008).
  - [32] M. Silva, V. Danos, E. Kashefi, and H. Ollivier, New J. Phys. **9**, 192 (2007).
  - [33] K. Fujii and K. Yamamoto, arXiv:0802.4137 (2008).
  - [34] S. Y. Looi, L. Yu, V. Gheorghiu, R. B. Griffiths, Phys. Rev. A **78**, 042303 (2008).
  - [35] W. Dür, H. Aschauer, and H. J. Briegel, Phys. Rev. Lett. **91**, 107903 (2003).
  - [36] K. Goyal, A. McCauley, and R. Raussendorf, Phys. Rev. A **74**, 032318 (2006).
  - [37] R. Raussendorf and H. J. Briegel, Phys. Rev. Lett. **86**, 5188 (2001).
  - [38] M. Van den Nest, A. Miyake, W. Dür, and H. J. Briegel, Phys. Rev. Lett. **97**, 150504 (2006).

- [39] M. Borhani and D. Loss, Phys. Rev. A **71**, 034308 (2005).
- [40] J. M. Taylor, J. R. Petta, A. C. Johnson, A. Yacoby, C. M. Marcus, and M. D. Lukin, Phys. Rev. B **76**, 035315 (2007).
- [41] Z.-R. Lin, G.-P. Guo, T. Tu, F.-Y. Zhu, and G.-C. Guo, Phys. Rev. Lett. **101**, 230501 (2008).
- [42] G.-P. Guo, H. Zhang, T. Tu, and G.-C. Guo, Phys. Rev. A **75**, 050301(R) (2007).
- [43] Y. S. Weinstein, C. S. Hellberg, and J. Levy, Phys. Rev. A **72**, 020304 (2005).
- [44] T. Tanamoto, Y.-X. Liu, S. Fujita, X. Hu, and F. Nori, Phys. Rev. Lett. **97**, 230501 (2006).
- [45] J. Q. You, X.-B. Wang, T. Tanamoto, and F. Nori, Phys. Rev. A **75**, 052319 (2007).
- [46] G. Chen, Z. Chen, L. Yu, and J. Liang, Phys. Rev. A **76**, 024301 (2007).
- [47] L.-M. Duan, E. Demler, and M. D. Lukin, Phys. Rev. Lett. **91** 090402 (2003).
- [48] J. J. García-Ripoll and J. I. Cirac, New J. Phys. **5**, 76 (2003).
- [49] O. Mandel, M. Greiner, A. Widera, T. Rom, T. W. Hänsch, and I. Bloch, Phys. Rev. Lett. **91**, 010407 (2003).
- [50] D. P. Aliferis and D. W. Leung, Phys. Rev. A **70**, 062314 (2004).
- [51] H. Wunderlich, C. Wunderlich, K. Singer and F. Schmidt-Kaler, Phys. Rev. A **79**, 052324 (2009).
- [52] M. A. Nielsen and I. L. Chuang, *Quantum Computation and Quantum Information* (Cambridge Univ. Press, Cambridge, UK, 2001).
- [53] D. Jaksch, H.-J. Briegel, J. I. Cirac, C. W. Gardiner, and P. Zoller, Phys. Rev. Lett. **82**, 1975 (1999).
- [54] M. Greiner, O. Mandel, T. Esslinger, T. W. Hänsch and I. Bloch, Nature **415**, 39 (2002).
- [55] C. Zhang, V. W. Scarola, and S. Das Sarma, Phys. Rev. A **75**, 060301(R) (2007).
- [56] M. Köhl, H. Moritz, T. Stöferle, C. Schori, and T. Esslinger, J. Low Temp. Phys. **138**, 635 (2005).
- [57] S. Stock, Z. Hadzibabic, B. Battelier, M. Cheneau, and J. Dalibard, Phys. Rev. Lett. **95**, 190403 (2005).
- [58] I. B. Spielman, W. D. Phillips, and J. V. Porto, Phys. Rev. Lett. **98**, 080404 (2007).
- [59] I. B. Spielman, W. D. Phillips, and J. V. Porto, Phys. Rev. Lett. **100**, 120402 (2008).
- [60] M. C. Garrett and D. L. Feder, New J. Phys. **10**, 033009 (2008).
- [61] M. S. Tame, M. Paternostro, M. S. Kim, and V. Vedral, Phys. Rev. A **72**, 012319 (2005).
- [62] T. P. Friesen and D. L. Feder, Phys. Rev. A **78**, 032312 (2008); J. Cho, Phys. Rev. Lett. **99**, 020502 (2007); J. Joo, Y. L. Lim, A. Beige, and P. L. Knight, Phys. Rev. A **74**, 042344 (2006).
- [63] C. Zhang, S. L. Rolston, and S. Das Sarma, Phys. Rev. A **74**, 042316 (2006); D. Schrader, I. Dotsenko, M. Khudaverdyan, Y. Miroshnychenko, A. Rauschenbeutel, and D. Meschede, Phys. Rev. Lett. **93**, 150501 (2004).
- [64] A. Kay, J. K. Pachos, and C. S. Adams, Phys. Rev. A **73**, 022310 (2006); T. Calarco, U. Dorner, P. S. Julienne, C. J. Williams, and P. Zoller, Phys. Rev. A **70**, 012306 (2004).
- [65] I. Bloch, Nature **453**, 1016 (2008).
- [66] S. Peil, J. V. Porto, B. L. Tolra, J. M. Obrecht, B. E. King, M. Subbotin, S. L. Rolston, and W. D. Phillips, Phys. Rev. A **67**, 051603(R) (2003).
- [67] Y. R. P. Sortais, H. Marion, C. Tuchendler, A. M. Lance, M. Lamare, P. Fournet, C. Armellin, R. Mercier, G. Messin, A. Browaeys, and P. Grangier, Phys. Rev. A **75**, 013406 (2007).
- [68] K. D. Nelson, X. Li, and D. S. Weiss, Nature Phys. **3**, 556 (2007).
- [69] K. D. Nelson, X. Li, and D. S. Weiss, Nat. Phys. **3**, 556 (2007).
- [70] Y. Miroshnychenko, W. Alt, I. Dotsenko, L. Förster, M. Khudaverdyan, D. Meschede, D. Schrader, and A. Rauschenbeutel, Nature **442**, 151 (2006).
- [71] L. E. Danielsen and M. G. Parker, Des. Codes Cryptogr. **49**, 161 (2008).
- [72] D. K. L. Oi, S. J. Devitt, L. C. L. Hollenberg, Phys. Rev. A **74**, 052313 (2006).
- [73] D. Gottesman, arXiv:quant-ph/9705052.